Article:

Nutter, J., Qi, J., Farahani, H. et al. (2023) In situ TEM observations of the growth of bainitic ferrite in an Fe-0.3C-3Mn-1.5Si-0.15Mo steel. Acta Materialia, 252. 118924. ISSN: 1359-6454

https://doi.org/10.1016/j.actamat.2023.118924

Acta Materialia 252 (2023) 118924

Contents lists available at ScienceDirect

Acta Materialia

journal homepage: www.elsevier.com/locate/actamat

In situ TEM observations of the growth of bainitic ferrite in an Fe-0.3C-3Mn-1.5Si-0.15Mo steel

John Nutter [a,*], Jiahui Qi [a], Hussein Farahani [b,c], W. Mark Rainforth [a], Sybrand van der Zwaag [d]

[a] Department of Material Science and Engineering, The University of Sheffield, Sir Robert Hadfield Building, Sheffield, S1 3JD, UK
[b] Tata Steel, Research & Development, IJmuiden, PO Box 10000, 1970 CA, the Netherlands
[c] Department of Materials Science and Engineering, Delft University of Technology, Mekelweg 2, Delft, 2628 CD, the Netherlands
[d] Faculty of Aerospace Engineering, Delft University of Technology, Kluyverweg 1, Delft, 2629 HS, the Netherlands

ARTICLE INFO

Keywords:
In situ transmission electron microscopy (TEM)
Steels
Phase transformation
Bainitic steel
Transformation kinetics

ABSTRACT

The current study reports in situ TEM observations of the growth of bainitic ferrite in an Fe-0.3C-3Mn-1.5Si-0.15Mo steel held isothermally at 300 °C with a higher spatio-temporal resolution than in previous studies. Significant variations were found in the lengthening rate, with the highest being in excess of 30,000 nm.s^{-1} while more common lengthening rates of 10–1000 nm.s^{-1} provided the highest quality observations. Both sheaves with visible sub units and individual laths were observed during growth with the lengthening behaviour of sheaves found to be discontinuous - in the most favourably oriented sheave this could be linked to sub unit behaviour. The transformation behaviour was comparable to that of HT-LSCM observations of bainitic ferrite growth for the most comparable steel compositions and to 'textbook' descriptions of the formation of bainite sheaves. In addition, other relevant phenomena were recorded, including the generation and movement of dislocations in the austenite during transformation, the interaction of laths with twin boundaries and the initially slow growth of bainitic ferrite laths.

1. Introduction

The austenite to bainite transformation has been the subject of ongoing research interest for many years due to the importance of bainitic steels in applications requiring properties such high strength and ductility, toughness, and creep resistance at reasonable costs [1–3]. Debate over the dominant rate controlling mechanism of bainite formation resulted in two alternative mechanisms proposed – a displacive and a diffusional approach. In the former, the nucleation is the rate controlling factor in bainite growth, whilst for the latter the diffusion of carbon limits interface mobility [4]. Both models have in common that the lengthening rates of the bainite may change with state of transformation but should be more or less equal irrespective of the position of the bainitic sheaf within the grain. Detailed observations at higher spatio-temporal resolution of the growth of bainite may help to establish the contribution of both processes in the overall transformation and also may establish whether the concept of the local transformation kinetics of bainite formation being more or less identical in every part of the grain is correct.

High temperature Laser Scanning Confocal microscope (HT-LSCM) to directly observe the bainite transformation has found increasing use in the metals research community [5–20], complementing more traditional methods such as (post mortem) metallography and dilatometry (not yielding morphological or local information). This relatively inexpensive technique has a number of advantages as it enables real time observation of bainite sheaves, allowing individual kinetic measurements, identification of probable nucleation sites and so on, but lacks a high spatial resolution and in the end remains a surface analysis technique.

Nevertheless, the transformations in binary Fe-C alloys [5], the Fe-C-Mn [6] and Fe-C-Ni systems [7,8], as well as alloys of more complex compositions [9–15], including superbainitic steels [16–20], have been investigated with this technique under a range of conditions including continuous cooling and isothermal holding. Under optimal conditions measurements of individual lengthening rates could be made and nucleation sites could be identified. In many studies nucleation was found to occur at grain boundaries, inclusions, existing sheaves, twin boundaries and in some cases within the grain with no apparent feature. In some, but not all, studies it was found that lengthening rates differed with the locally active nucleation site.

* Corresponding author.
E-mail address: j.nutter@sheffield.ac.uk (J. Nutter).

https://doi.org/10.1016/j.actamat.2023.118924
Received 26 October 2022; Received in revised form 30 March 2023; Accepted 8 April 2023
Available online 9 April 2023

In contrast, the use of hot stage Transmission Electron Microscopy (HS-TEM) to study the bainite transformation is limited. Nemoto [21] performed an early experiment in an Fe-Ni-C alloy using high voltage electron microscopy and observed the growth of acicular and non-acicular bainite grains at temperatures below 500 °C. Kang et al. [22] observed bainite growth during isothermal holding in four steels, an iron alloy and two copper alloys.

Previously, however, HS-TEM has been successfully used to make both qualitative and semi-quantitative observations of phase transformations and other dynamic behaviour in a range of alloys including steels. Darken and Fisher [23] made early observations of the formation of pearlite in evaporated thin films of eutectoid steel. Purdy directly observed ferrite formation and the transformation dynamics in Fe-C-Mo and Fe-C-Si steels [24,25], Du et al. studied the dislocation behaviour associated with austenite growth from delta ferrite [26]. Onink et al. [27] and Nutter et al. [28] found overall transformation behaviour consistent with that found in calculation or bulk experiments for the austenite to ferrite transformation in Fe-C and Fe-C-Mn steels.

The use of TEM provides several advantages, including higher magnification which brings an improved ability to observe substructure and the potential to observe any dislocation behaviour in real time. The use of thin electron transparent specimens allows observers to be confident that they have recorded all behaviour throughout the thickness of the sample, in contrast to LSCM experiments where lengthening rates and other observations could be affected by the direction of growth with respect to the free surface [8].

In this study we report observations of bainitic growth under isothermal conditions, recording nucleation position and lengthening behaviour. A small number of observations were also made during cooling to the holding temperature. The additional resolution provided by TEM allowed observation of the development of individual sheaves with non-linear lengthening behaviour. In addition we note the variety in the appearance and lengthening rates of the growing bainitic ferrite between different observations - even within individual austenite grains. The in-situ TEM measurements are complemented with subsequent AFM measurements and automated crystal orientation mapping to deepen the interpretation of the observations.

2. Experimental methods

A steel with a composition of Fe-0.3C-3Mn-1.5Si-0.14Mo was selected for observation due to relatively slow transformation kinetics and because of the role of Si in suppressing carbide formation under paraequilibrium growth conditions [29]. The preliminary dilatometric studies, shown in Fig. 1, indicated that at temperatures between 300 and 350 °C the transformation takes 1 to 2 h, which makes it possible to record the transformation in a TEM equipped with a fast camera and suitable image capture and storage facilties with a much higher spatio-temporal resolution than was obtained in previous studies.

Specimens were prepared for hot stage TEM experiments by sectioning and mechanically thinning to approximately 100 μm. 3 mm discs were punched out from this material and electropolished in a Struers TenuPol-5 electropolishing unit at −40 °C with a 5 pct perchloric acid, 35 pct 2-butoxyethanol, 60 pct methanol solution. Ideally, specimens require a smooth central perforation to minimise tearing of the foil during heating and cooling as well as possessing a large electron transparent region due to thickening of the foil edges during heat treatment [30].

Hot Stage TEM experiments were carried out using a GATAN model 628 single tilt heating holder with a Ta furnace and a model 628.09 J water re-circulator which was switched on 20 min before the heat treatment began. Temperature control was carried out using the temperature ramping function and manually reducing the temperature after austenitisation.

The majority of observations were carried out in a JEOL JEM-F200 TEM operated at 200 kV and equipped with cold field emission gun. A

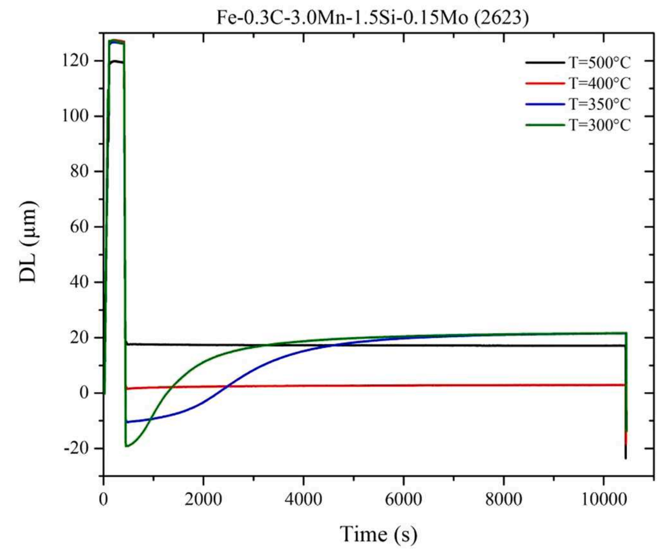

Fig. 1. Length change of specimen measured by dilatometry. At 300 °C, the transformation progresses over period of up to 3600–7200 s.

GATAN Oneview IS camera was used to record both still and live images of the transformation, with the video recording at 25 frames per second (0.04 s exposure time per fame). In addition, a JEOL JEM 3010 UHR TEM operated at 300 kV, with a LaB6 filament was used for early observations. In this case video was recorded using the attached TVIPS camera with a 100 ms exposure time for individual frames. Thickness measurements were made using EELS [31], using a GATAN Quantum GIF attached to the JEM-F200, operated in STEM mode, probe size 4, a 40 μm condenser aperture and a camera length of 150 mm. Under these conditions the convergence semi-angle, α, was 5 mrad and the collection semi-angle, β, was 12 mrad. These indicated that the thinnest regions of the foil were in excess of 150 nm after heat treatment, increasing to approximately 350–400 nm at 20 μm from the foil edge. All observations were made within 20 μm of the edge, with the majority 5–10 μm from the hole for which the estimated thicknesses were 250–300 nm. Post heat treatment EDS showed a depletion of Mn in the foil, with the lowest levels of Mn measured in the thinnest regions of the foil. In the thinnest regions the foil contained 0.5–1 wt.% Mn compared to 1.8 wt.% Mn in the thickest electron transparent regions.

A total of 10 video clips were recorded showing the growth of one or more bainitic ferrite plates, 8 during isothermal holding and 2 during cooling. Two further clips show the growth of bainitic ferrite during reheating.

Figure 2 shows the two heat treatments to which the specimens were subjected. Specimens were heated to 1000 °C at 200 °C/min and held for 5 min before cooling to 300 °C. The average cooling rate achieved was −18.5 °C/min, but was significantly higher in the initial stages of cooling, between 1000 °C and 600 °C, where the average cooling rate was −44 °C/min. In preliminary experiments this thermal profile was found to result in much of the electron transparent region having transformed into allotriomorphic ferrite making observation difficult. A larger austenite grain size increased the chances of finding untransformed austenite and successfully observing the transformation at 300 °C. It is well established that grain growth is inhibited in thin foil specimens due to surface effects and little to no austenite grain growth was observed in the present experiments [32–34]. Therefore a second cycle – identical to the first – was performed, producing a coarser austenite microstructure and more consistently obtain the desired transformation. This coarsening was possible due to the fact that the microstructure after the first cycle was not as fine as the starting microstructure, reducing the available nucleation sites for austenite on reheating. Examination of the foil during isothermal holding and after

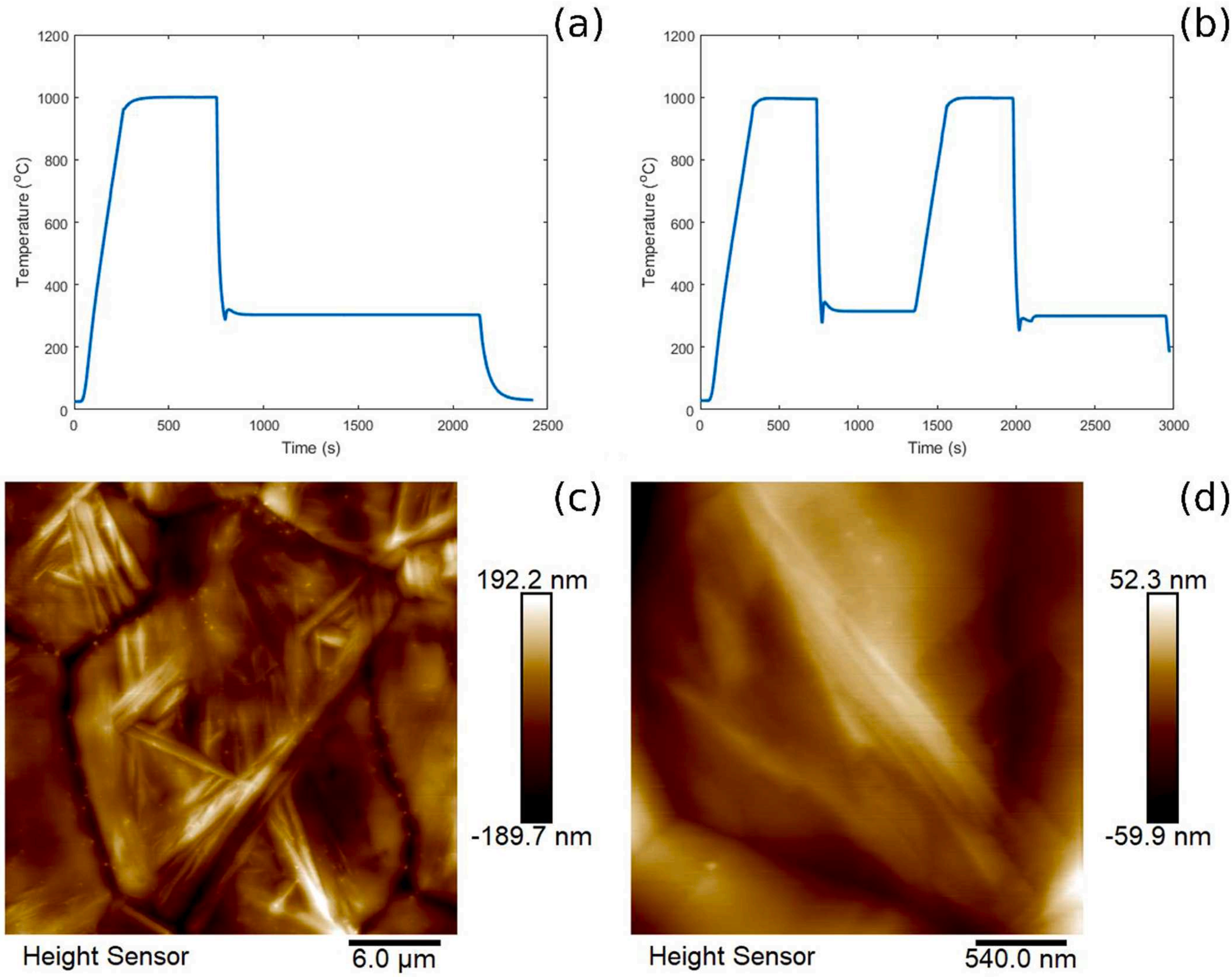

Fig. 2. (a) Single cycle heat treatment (b) Two cycle heat treatment (c) AFM height image showing the surface relief due to the transformation away from the central perforation of the thin foil and (d) AFM height image showing the transformation close to the central perforation of the thin foil. In both (c) and (d) the surface after the full two cycle treatment is shown.

heat treatment indicate that whilst a significant volume had transformed to allotriomorphic ferrite, there were numerous regions that had undergone the transformation to either Widmanstätten or bainitic ferrite.

AFM on TEM samples which had been subjected to the full heat treatment outlined in Fig. 2(b) was carried out using a Bruker Dimension XR AFM in the liquid cell. Bruker's sharp Nitride Lever (SNL) probes with a normal tip radius of 2 nm and low spring constant (0.06 N/m) were used. The samples were kept in the methnol all the time to avoid oxidation. This technique was to confirm that the transformation in the thin regions contained a shear component. Figure 2(c) shows the surface of the transformed thin foil measured away (>100 µm) from the electron transparent region. Figure 2(d) shows the height measured within 20 µm from the edge of the central perforation. In both cases austenite grain boundaries are picked out through thermal grooving and it can be seen that the grain size is refined in the thinner regions due to the inhibition of recrystallisation and grain growth when the thickness of the foil is less than the diameter of the grain. In both cases the transformed bainite is visible on the surface. Figure 2(c) qualitatively resembles the profiles found within the literature for silicon containing steel transformed at 200 and 350 °C [35,36]. The thinner region in Fig. 2(d) is less clear because of greater curvature of the surface but likewise shows that the transformation resulted in surface relief due to the shear component. Calculated apparent shear was comparable for both regions at approximately 0.13, which is comparable to the values found by Peet and Bhadeshia [36].

Post heat treatment diffraction analysis was carried out using the NanoMEGAS ASTAR automated crystal orientation mapping (ACOM) system. This uses precession electron diffraction to generate EBSD like data [35,36] and was used to confirm the phase and identify the orientation of laths and grains recorded during isothermal holding. A precession angle of 0.7° was used, with step sizes of 10–20 nm.

3. Results

The primary observations reported here are of the growth of bainitic ferrite during isothermal holding. A small number of transformations were captured in situ during cooling. Previously transformed regions could be seen during isothermal holding but it was difficult to capture this transformation on video due to the high cooling rate and the effect of this on specimen drift and focus. Figure 3 shows selected frames from the growth of Widmanstätten ferrite and bainite growth. Initially, the growth of ferrite was observed from approximately 700 °C (Fig. 3(a)),

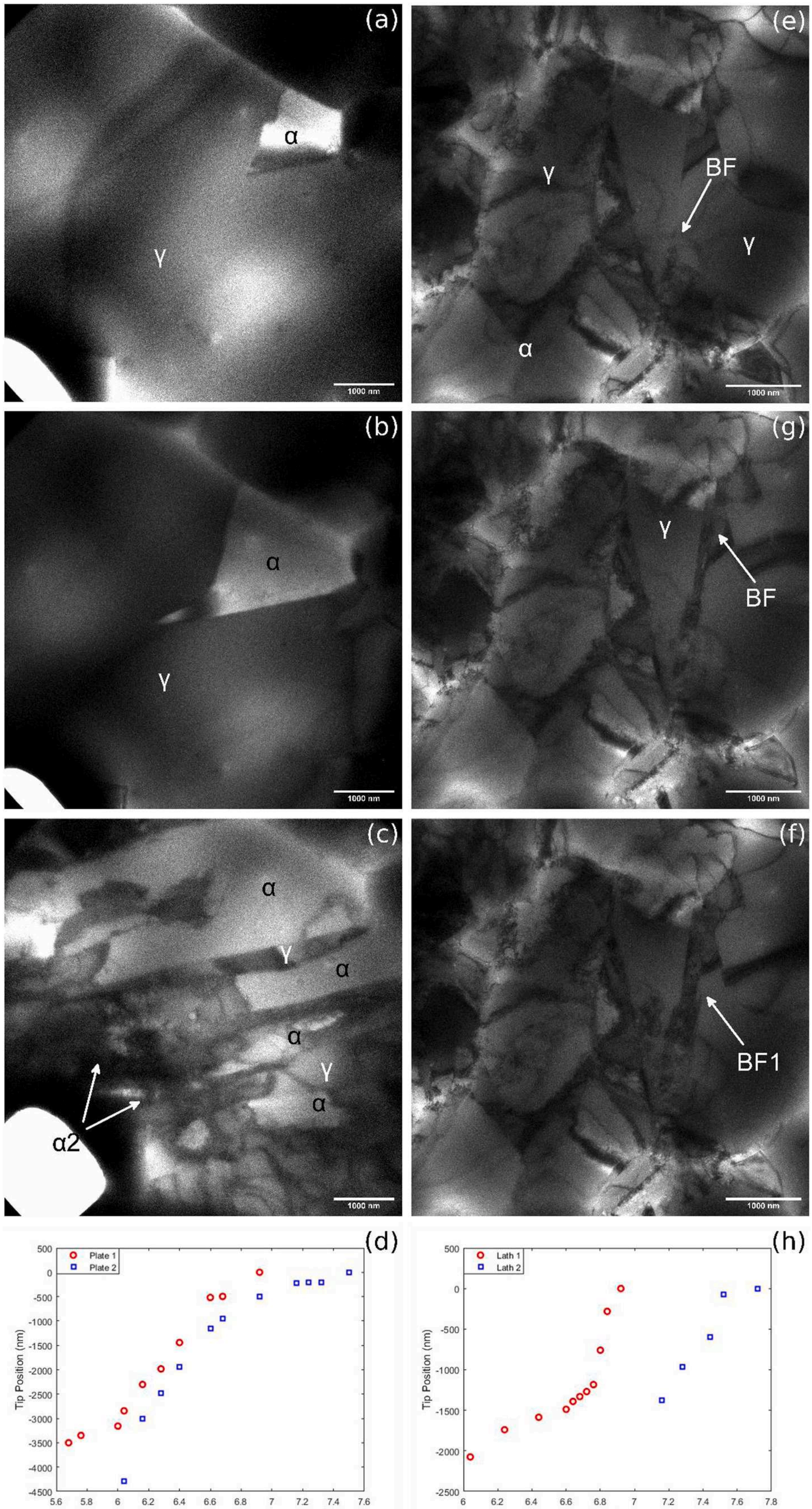

Fig. 3. (a–c) BF TEM of Widmanstatten growth at 5, 6.12 and 10.03 s after the temperature was lowered, (d) Tip position against time for the two Widmanstatten ferrite plates that were completely within the field of view, (e–f) BF TEM of Bainitic ferrite growth at 6.2, 6.88 and 7.44 s after the temperature was lowered, (h) Tip position against time for the two identified laths.

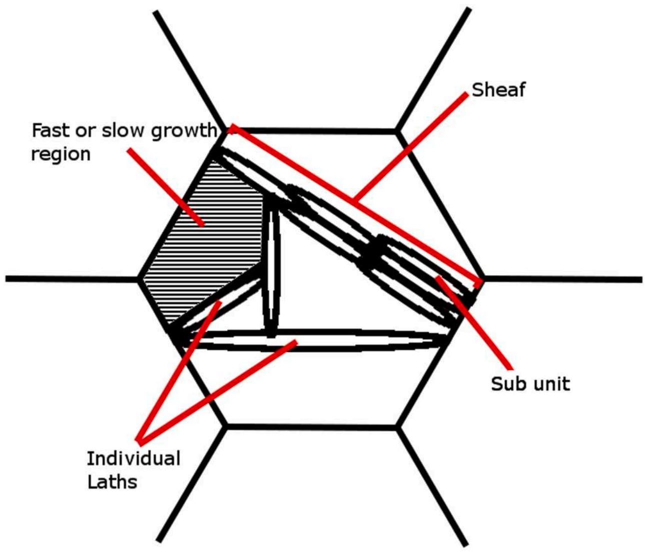

Fig. 4. Schematic representation of different growth behaviours in the bainitic ferrite. Sheaves with an appearance close to that found in the literature were identified with the growth of the constituent subunits also seen visible. In addition laths were observed to grow individually, not forming part of any apparent sheaf. Finally, several regions transformed at a rate that made classification difficult due to fast or slow transformation rate.

taking on a definitive Widmanstätten appearance at approximately 635 °C (Fig. 3(b)). This was followed by the growth of more heavily dislocated laths resembling bainite which were observed to grow into in the untransformed austenite once the temperature reached approximately 582 °C (Fig. 3(c)).

The ferrite can be seen to nucleate on a grain boundary triple point, with the two sides close to the [011] and [002] directions. Initially one face grew through the propagation of large ledges (one such is visible in Fig. 3(a)). One of the plates grows from a perturbation in the existing ferrite grain. Initially this perturbation has a “wedge” (i.e. like 3 sides of a trapezium) shape before converting into the needle like morphology visible in Fig. 3(b). Subsequently, this and other Widmanstatten ferrite plates grew across the field of view. After lengthening had terminated, it was possible to see that the remaining untransformed austenite between the plates was backfilled (that is, with a growth direction opposite to that of the ferrite plates) with a more heavily dislocated phase resembling bainite, as in Fig. 3(c). Figure 3(d) shows the tip position against time for the 2 plates that were fully within the field of view whilst transforming. The two plates evolve in a similar manner with lengthening rate proportional to $t^{-1/2}$.

Bainitic ferrite growth was also observed during the continuous cooling at approximately 380–370 °C, shown in Fig. 3(e-g). Figure 3(h) shows the tip position against time for the initial lath and a second lath which was also observed to grow parallel to it. The original lath had a readily apparent discontinuity in lengthening behaviour – rapidly increasing in the final stages of the transformation. The average lengthening rates for the two laths are 2.2 and 4.1 μm.s^{-1} respectively with the highest instantaneous growth rates measured as 11.9 and 6.6 μm.s^{-1}.

Observations of bainite growth during isothermal holding revealed some variation in the appearance and behaviour of the growing phase. Bainite growth that appeared to closely match textbook descriptions of the nucleation and growth of subunits in a single sheaf was observed. Alongside the sheaf observation, the growth of other laths, both individually or near and parallel to existing laths, was also recorded. In addition, multiple regions were observed to completely transform within the space of a single frame indicating very high lengthening rates (in excess of 30 μm.s^{-1}) and the nucleation of multiple plates within a very short space of time (typically less than 0.04 s). In other cases transformation was so slow (down to a minimum average growth rate of 2 nm.s^{-1}) that the transformation could only be seen through a series of time lapse images. In both cases, this makes it difficult to classify the growth behaviour in the same way as those transforming at intermediate rates. Figure 4 schematically illustrates the differences in appearance between the observed growth modes. Some typical examples of this behaviour, that are not depicted in other figures, are shown in Fig. 5 below. Figure 5(a&b) shows very slow growth of bainite, whilst Fig. 5(c) shows the growth of a pair of bainitic ferrite laths in which one was observed to grow across (i.e. above or below within the foil) the other. Figure 5(d) shows the average apparent lengthening rate for the bainitic ferrite during isothermal holding – most measurements fell within the 100–1000 nm.s^{-1} range, with some examples of very rapid or very slow growth behaviour. In addition to the order of magnitude differences in average lengthening rate, the bainitic ferrite also displayed differing growth behaviour in that some grew linearly whilst others displayed discontinuities – this is discussed in more detail below. These different growth rates and bainite morphologies often coexisted within a single sample and within a single austenite grain.

Where possible, the thickness of the sheaves or laths was measured at the mid-point immediately after lengthening was completed and is shown in Fig. 5(e), with most measurements falling in the range of 20–150 nm and a small number displaying higher average thicknesses. Further breaking these down by type shows that the higher thickness measurements were predominantly from identifiable sheaves, whilst individual laths had comparable thickness at this stage to those laths which formed a subunit of a larger sheaf.

Where possible the likely nucleation position of the bainite sheaf was noted. In some cases it was either not possible to determine the nucleation position with confidence. Of those that could be attributed with confidence, 10 laths were observed to nucleate on grain boundaries, 4 on twin boundaries within the austenite and 4 on existing bainitic ferrite laths. No nucleation was seen within the austenite grain not showing crystallographic defects or interfaces. It should be noted that for the purposes of defining the nucleation of a new lath on an existing lath, this was only included when the growth direction was significantly different. As outlined below it was possible to see the development of subunits which nucleated on an existing lath and shared approximately the same growth direction, which are not included.

Two additional observations are worth highlighting. Firstly, for all nucleation on grain boundaries and existing laths there are examples of nucleation close to where an existing lath intersected the position. Nucleation of new laths occurred at both the positions where the existing lath had previously nucleated as well as where growth had been halted by impingement. Secondly, where a lath was observed soon after nucleation, initial growth was slow before rapidly increasing. Figure 6 shows the tip position against time for one individual lath and one clearly distinguishable subunit that were observed sufficiently early. Similar behaviour was observed for the sheaf depicted in more detail in Fig. 7. The acceleration of the growth rate occurred at the tip having moved approximately 150–250 nm in three cases.

Figure 7(a–e) shows the lengthening of a single bainite sheaf, with behaviour that is typical of textbook descriptions of the process. Fig. 7(f) plots the tip position of the sheaf as a whole, and the length of individual subunits where these could be measured. The lath is first observed after nucleating on an existing bainitic ferrite sheaf, when it had a measured length of approximately 100 nm. Growth was initially slow as with the laths in Fig. 6, before increasing at approximately 180 nm. Growth was then inhibited at approximately 1300–1400 nm. At this stage a first subunit becomes apparent which grew until it reached approximately the tip of the existing lath. Once this occured rapid lengthening of the sheaf continued. From Fig. 7(d) it can be seen that the growing tip of the sheaf is not the same thickness as the combined thickness of the original lath and the first subunit, indicating that growth was resumed either by the nucleation of a new subunit at the tip of the sheaf or by the renewed

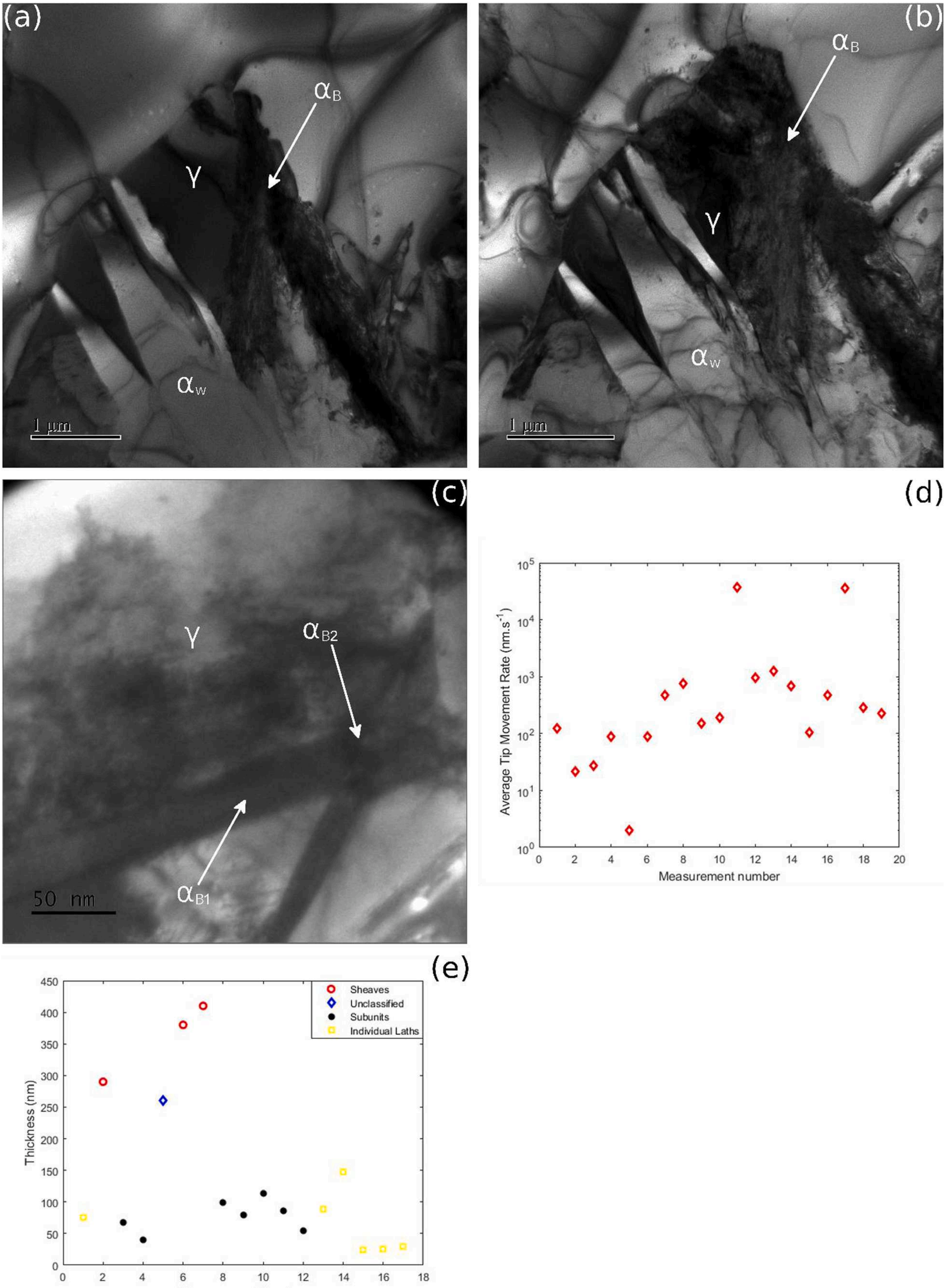

Fig. 5. (a&b) BF TEM of slow growing bainite after isothermal holding for 1690 and 3150 s respectively. (c) Bainitic ferrite laths which were observed to cross during growth, indicating that the laths had not penetrated through the full thickness of the foil. (d) Average tip movement rate for each of sheaf or individual lath. (e) A comparison of thickness for sheaves, individual laths and subunits immediately after lengthening was completed.

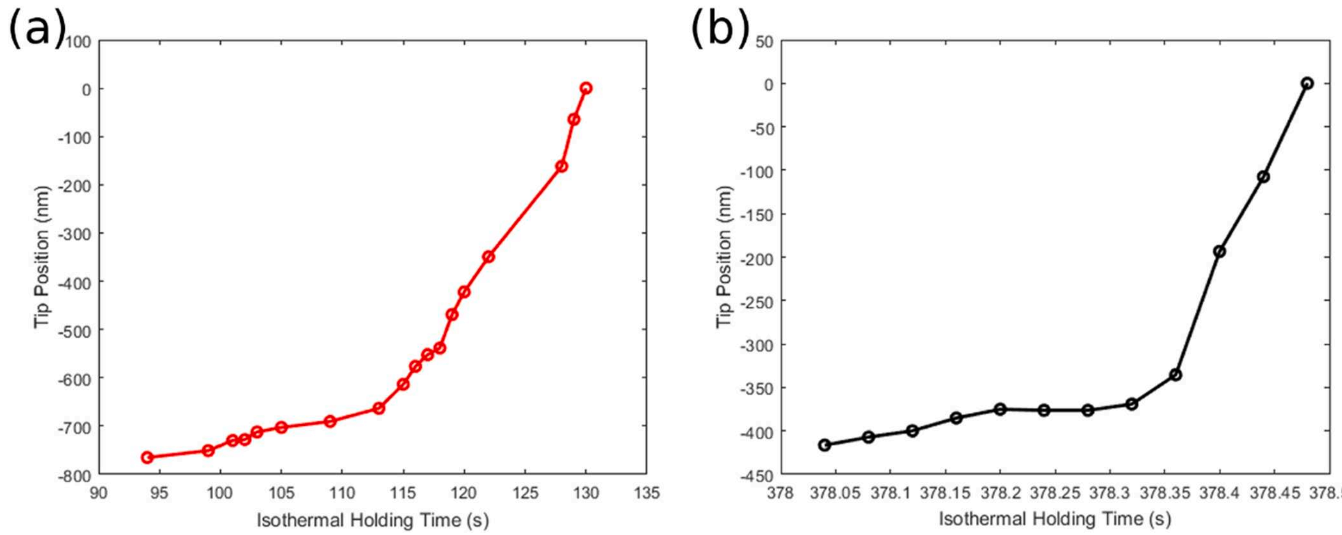

Fig. 6. Tip position against isothermal holding time for (a) A sub unit and (b) an individual lath.

growth of the original lath. Lengthening is ultimately halted by the impingement of the growing sheaf on an existing bainite lath. Note also that there is some observable overlap of the two sheaves indicating that the bainitic ferrite did not form throughout the entire thickness of the foil.

Subsequently, three additional subunits are seen to grow along the sheaf. Unexpectedly one of these subunits grows backwards towards the nucleation position. Fig. 7(f) shows that the overall lengthening rate for the sheaf is slower as a result of the growth stasis with an average of 100 nm.s^{-1} compared to an average of 450 and 400 nm.s^{-1} for the two rapid periods of lengthening.

Figure 8 shows the transformation in the same austenite grain before and after that shown in Fig. 7, and demonstrates that even within the same austenite grain the apparent behaviour of the developing laths was often variable. A total of 6 bainitic ferrite growth events were observed in this grain with the sheaf displayed in Fig. 6 now being designated as BF 5.

BF 1 was the most difficult to observe due to local contrast conditions. Growth appears as a single broad lath which continues until it impinges on the austenite grain boundary. Initially there appears to be little migration of the lath, as seen in Fig. 8(a), for the first 12 s of observation, after which more easily observable lengthening occurs. Subsequently two subunits nucleated at approximately 1/3 of the way along the initial length, with one each growing along the positive and negative directions of growth. A third, just visible, subunit appears to grow along the top of the original lath. Thus BF 1 is considered to be similar to the textbook case of BF 5 but with less favourable contrast conditions and orientation of new subunits.

BF 2 nucleated at a position adjacent to the nucleation position of lath 1 (seen shortly after in Fig. 8(b) and in supplementary video 2). BF 2 did not display any clearly distinguishable subunits as in the previous cases and maintained a rectangular appearance. Although it more obviously resembled austenite annealing twins, the ferritic nature of the lath/sheaf was confirmed using electron diffraction after the transformation had ended. In addition thickening of the sheaf was noted during the observation period and at no time was similar behaviour observed in confirmed annealing twins during the present hot stage TEM experiments. A further interesting feature of this sheaf/plate is that the tip is broad with periodic appearances of ledge/steps. Thus, lengthening proceeds through periods of general lengthening interspersed with periods where steps form with one step apparently inhibited in its growth relative to the other (Fig. 8(b-c)). Generally the top step represented the leading edge but this was not always the case. The transformation of BF 3 was not captured on video but can be seen from Fig. 8(d) onwards, it is notably narrower than the other laths. BF 4 appears to be made up of parallelogram shaped subunits which rapidly nucleate on the left-hand side corner of the previous unit as shown in Fig. 8(d-e).

Finally, BF 6 (Fig. 8(f-g)) began growing at the junction of BF 2 and 4. This began relatively slowly but after growing to approximately 750 nm the growth rate rapidly increased with a larger area rapidly transforming to bainitic ferrite. This represents an example of the extremely rapid (within 1 frame or 0.04 s) transformation. Approximately half of the austenite in a parallelogram shaped area bounded by BF 1–4 transformed with an estimated lengthening rate in excess of 37 μm.s^{-1}. Therefore, we can conclude that within a single austenite grain multiple apparently distinct types of behaviour were observed.

During growth of bainitic ferrite it was possible in some cases to observe the presence and behaviour of dislocations and their relation to the moving transformation front. Due to the relatively rapid nature and unpredictable position of the observed transformation, it was not possible to (pre-)tilt the sample to ideal contrast conditions for the observation of dislocations – therefore, whilst it is possible to report actually observed dislocation behaviour, the absence of visible dislocations is not taken to indicate the absence of dislocations in the material. In some cases the growing tip resulted in the generation of new dislocations, an example of this can be seen in Fig. 7(a-b). Generally, those which remained in contact with the bainitic ferrite appeared predominantly immobile, whilst some movement was seen for those which were not. Finally, dislocation generation and movement was seen in several cases before the appearance of a lath, potentially corresponding to the nucleation of the lath or its very early stages of growth, as well as in the immediate aftermath of completed lengthening. Supplementary Video 3 shows this most clearly where an avalanche of dislocation activity was observed after the lengthening of a baintic ferrite lath. The movement of dislocations ahead of a growing bainitic ferrite lath is shown in Supplementary Video 4.

One additional feature observed was the growth of bainite laths across twin boundaries. Figure 9 shows a sequence of BF TEM images showing growth across a twin boundary accompanied by a deflection in the growth direction. The growing lath is once again deflected when the lath reaches a second twin boundary. Post heat treatment diffraction analysis determined that the orientation of the transformed bainitic ferrite remained the same with respect to the electron beam. When the third "clone" reached the end of the twin the lath did not continue to grow on the other side of the boundary. Although more difficult to observe (see Supplementary Video 4) it appears that the bainitic ferrite was reflected from this boundary growing for a short distance until growth finally terminates at a fourth twin boundary (Fig. 9(e)). In

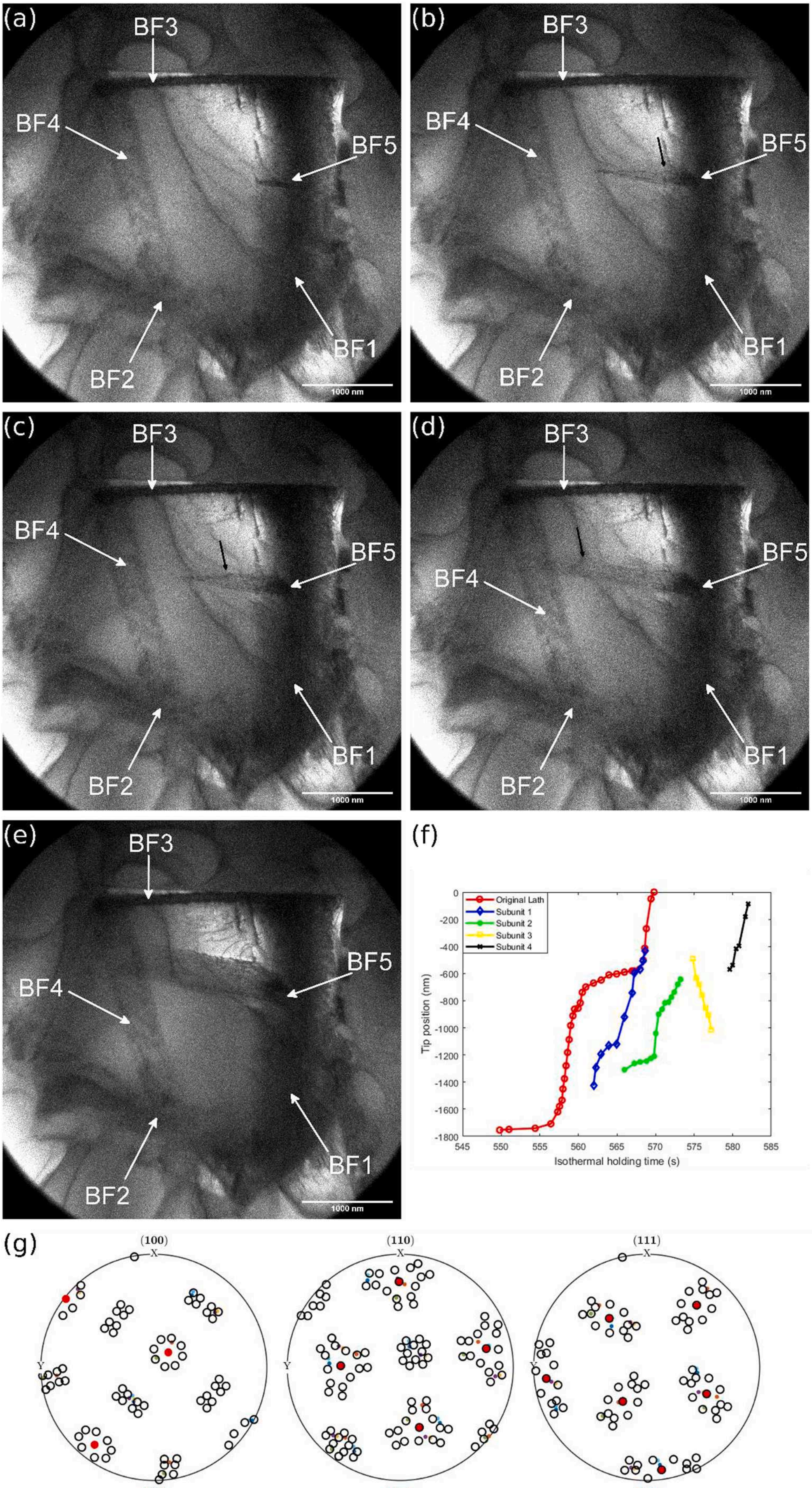

Fig. 7. BF TEM showing the progress of the transformation for the bainitic ferrite sheaf which displayed "textbook" growth behaviour after isothermal holding times of (a) 558 s (b) 561.96 s (c) 564.96 s (d) 569.4 s and (e) 583.2 s. Black arrows indicate the tip of subunit 1. (f) Tip position against isothermal holding time and (g) Pole figures constructed from ACOM data. The large red dot is the parent austenite orientation and the small, coloured dots the bainitic ferrite laths. The KS variants are shown by the black circles. The transformation of this sheaf is captured in Supplementary Video 1.

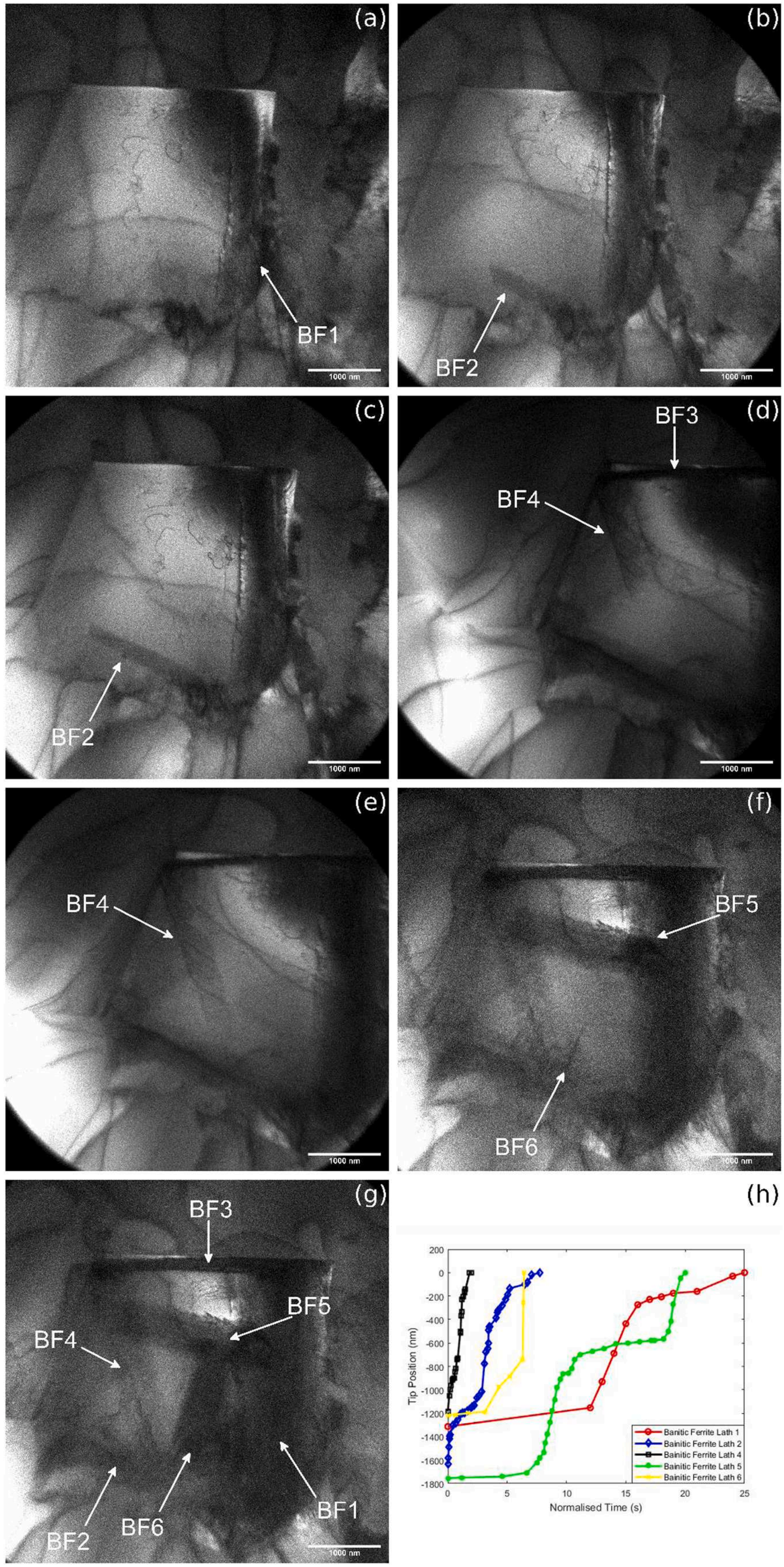

Fig. 8. (a–g) BF TEM images showing the development of the microstructure after isothermal holding for 166, 253, 254.12, 531.96, 532.72, 673.8 and 674.52 s. (h) Tip position against normalised time for laths 1,2,4,5 and 6.

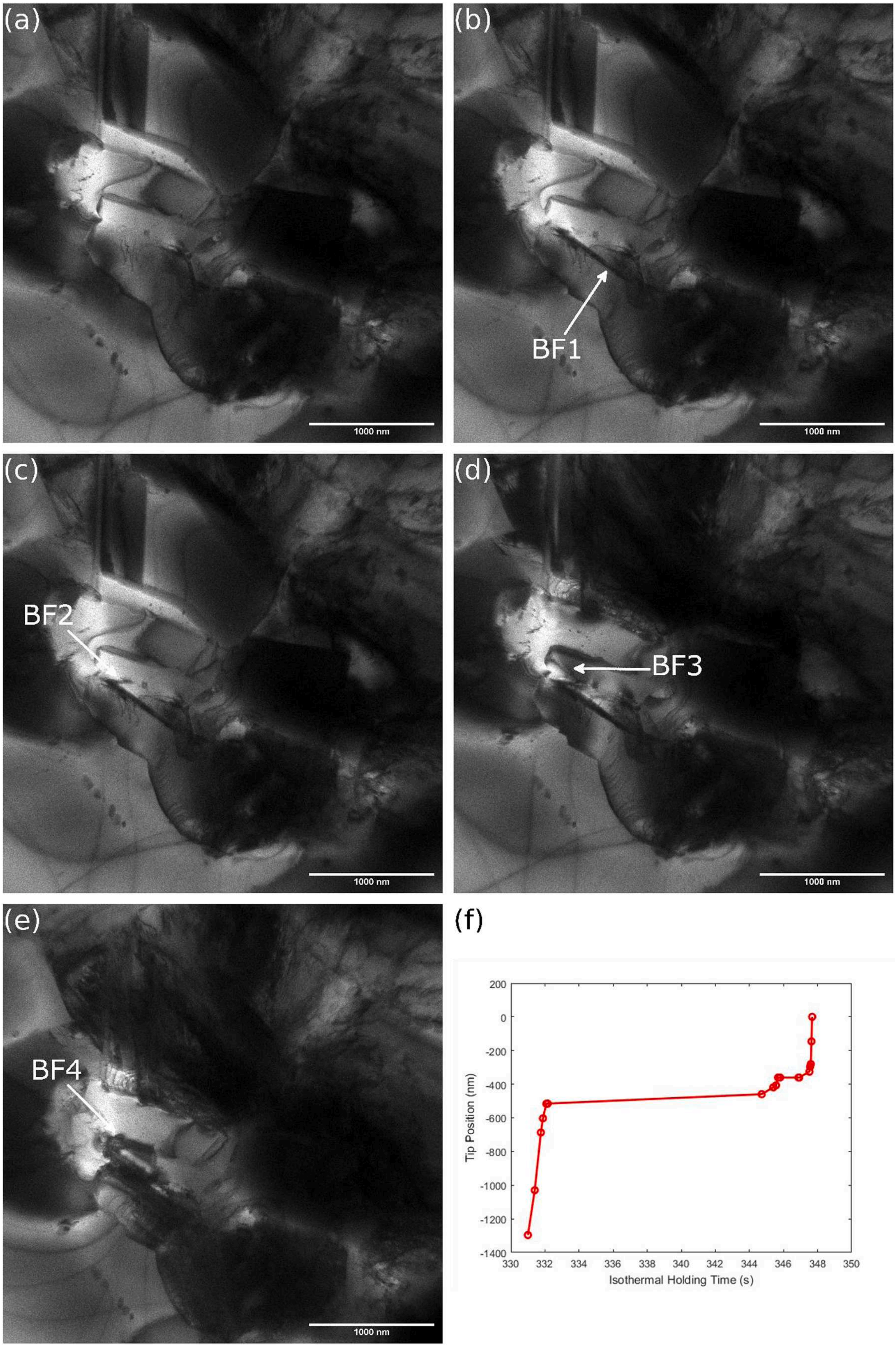

Fig. 9. (a-e) BF TEM of the growth of a bainitic ferrite lath across twin boundaries and the resulting deflection in growth direction after isothermal holding for 331, 344, 346, 348 and 586 s. (f) Tip position against isothermal holding time.

addition, the video indicates that there is a localised bending of the foil in the austenite side of boundary 3 made visible through expanding bend contours centred on the intersection between the bainitic ferrite and the boundary. Fig. 9(f) plots the total length of the lath and shows a lengthy (~12 s) period of stasis before growth continues on the other side of boundary 1. The stasis when the lath reaches boundary 2 is significantly shorter (<2 s). There is some variation of the lengthening rate at each stage with the first stage being the highest at 670 nm.s^{-1}, the second the slowest at ~100 nm.s^{-1} before increasing again in the thirst stage to 470 nm.s^{-1}.

4. Discussion

4.1. Nucleation

Prior in situ LSCM studies reported in the literature have been able to identify several nucleation sites in the bainite transformation. The primary observed locations are austenite grain boundaries, existing sheaves/plates, inclusions and nucleation events within the grain. In the present observations we identify 3 locations – austenite grain/interphase boundaries, twin boundaries, and existing sheaves. Although only a limited number of sites could be identified in comparison to LSCM studies, principally due to the narrower field of view, in these there was a preference towards grain boundaries (10 of the 18 nucleation sites) which is in agreement with some studies [12] . Interestingly, in many of the observed bainite growth events which originated at grain boundaries the position along the boundary was very close to where an existing sheaf intersected the boundary. Whilst nucleation at twin boundaries is somewhat unexpected due to the low interfacial energy [37,38], Mao et al. [10] made similar observations of nucleation sites of this type for transformations that occurred at lower temperatures (approximately 362 °C). Where it could be determined, the orientation relationship was close to the Kurdjumov-Sachs orientation relationship, as expected for bainite [39].

Where laths could be observed soon after formation, these were found to undergo initially slow growth before beginning to lengthen more rapidly. This would agree with observations of bimodal subunit size by Olsen et al. [40] in Fe-0.43C-3Mn-2.12Si steels isothermal transformed at 286 °C. Whilst the number of observations is small, we note that there was consistency between the initial and subsequent lengthening rates when comparing between instances of this behaviour. That is, the lath that was observed to lengthen fastest in the slow initial stage subsequently lengthened fastest, whilst the initially slowest growing lath subsequently lengthened at the slowest rate. This may indicate that the initial growth behaviour is influenced by the overall transformation kinetics. Such an inverse correlation between growth rate and nucleation time has also been observed in a LCSM study [12].

4.2. Lengthening behaviour

We report significant variation in the lengthening behaviour of observed bainitic ferrite during isothermal holding. Hu et al. (2014) [19] and Hu et al. (2015) [20] made observations at 330 °C on a Fe-0.4C-2.8Mn-2Si steel which is the most compositionally similar to the steel used here. Average sheaf growth rates are reported as 5.8 μm.s^{-1} by Hu et al. For similar conditions Hu et al. (2014) report average growth rates in the range of 1–5 μm.s^{-1} (depending on nucleation site) during cooling with lower lengthening rates during isothermal holding in the range of 0.35–0.62 μm.s^{-1}. Tian et al. [16], in steels of a similar composition to those studied here, report similar lengthening rates in the 430–330 °C cooling range of approximately 4 μm.s^{-1}.

We captured a single video recording of bainite transformation during continuous cooling where high quality measurements could be obtained, primarily due to the difficulties associate with choosing the correct field of view prior to the transformation and due to specimen drift during cooling. The average lengthening rate, at a start temperature of 370 °C, was 2.2 μm.s^{-1} and 4.1 μm.s^{-1}, for the first and second observed laths respectively. During isothermal holding sub 1 μm.s^{-1} average lengthening rates were typical. Therefore, there is reasonable agreement in lengthening rates between the present study and the most similar available in the literature, indicating minimal influence of the more constrained specimen dimensions required for in situ TEM compared with HT-LSCM.

A contrast between these studies and the present observations, however, is that differences are not simply between laths/sheaves, even within the same austenite grain, but that individual sheaves show clear periods of stasis or inhibited growth resulting in an overall lower average lengthening rate. In BF 5 above, for example, the average overall lengthening rate is approximately 25% of that for the periods of more rapid growth. The three studies (Hu et al. 2014, Hu et al. 2015 and Tian et al.) do not explicitly report stasis in the lengthening of individual sheaves, although Hu et al. (2014) note that lengthening was not constant during isothermal holding [19].

Comparing with the existing literature where the uniformity of the lengthening rate is explicitly noted, Yada et al. [7] found good linearity in Fe-Ni-C steels isothermally transformed between 230 and 500 °C. The length measurements of Sainis et al. [12] show variation in the lengthening rate for some bainite plates during isothermal transformation of an Fe-0.2C-1.5Mn-2.0Cr alloy at 410 °C, whilst others were linear or nearly linear. Hu et al. (2021) [13], for Fe-0.38C-1.44-Si-0.82Mn-0.90Cr-0.25Mo-0.08 V steel held isothermally at 410 °C, report clear periods of stasis which they associate with impingement of growing plates, with close to linear lengthening of plates outside of these periods. Furuhara et al. [8] report a linear relationship between length and holding time in Fe-C-9Ni steels transformed at 623–773 K but note some cases where the growth rate varied over a short time scale. Measured average growth rates between different laths/sheaves in these studies vary considerably and it is likely that intermediate rates are more conducive to sampling rates which reveal discontinuities in growth rate. The non-linearity reported by Sainis et al. and Furuhara et al. are most apparent in measurements where the bainite grows over a period of seconds to tens of seconds, rather than cases where the lengthening is completed within a few frames or where lengthening takes place over hundreds of seconds. It is possible that the apparent difference in apparent behaviour is non-physical but due to the limited spatio-temporal resolution of the LSCM.

Generally, the higher resolution associated with TEM observations would also contribute to the more accurate determination of the position of the growing tip compared to confocal experiments and therefore be more sensitive to discontinuities in the lengthening behaviour. In fact, the growth of bainite by the nucleation and growth of subunits would be expected to produce nonlinear lengthening of a sheaf – especially in cases where the growth of subunits is considered to be faster than the growth of the sheaf.

Several distinct kinds of growth behaviour were observed. In addition to the textbook example of a growing sheaf, as for BF 5 above, there were other sheaves which displayed similar behaviour but with a nucleation position of the subunits less favourable for observation, as for BF 1. In contrast, BF 4 appears to grow in a manner that appears to be consistent with some descriptions of lower bainite growth where the lengthening of the sheaf proceeds by nucleation of additional parallelogram shaped subunits at the broad face of the previous subunit [22,41]. In other cases individual laths were observed, often developing in parallel, which is a similar mechanism, on a smaller scale, to that reported by Mao et al. [10]. Whilst other observed transformations were too fast or too slow to classify, there are commonalities with the behaviour observed by Sainis et al. [12] who report differences in growth rate of a least 20 times between the fastest and slowest plate growing within a single austenite grain.

One other aspect of the observed lengthening behaviour bear some relevance to the growth stasis observed by Hu et al. (2021) [13], which is attributed to the formation of a new nucleus rather than growth continuing below the surface. Although no nucleation of this kind was observed, our observations do show the unambiguous transmission of a growing bainitic ferrite lath across a twin boundary which was oriented parallel to the electron beam – no comparable observations are reported in LSCM experiments to our knowledge. This features an apparent stasis period as the twin boundaries are crossed, similar to the growth stasis of Hu et al. Interestingly, the stasis period varies as the lath crosses different boundaries, despite the fact that these boundaries are of the same nature and orientation with respect to the lath. It is not immediately apparent from the observations what gives rise to this difference in the stasis period, although the length of the lath segment, and the volume of austenite between each twin boundary does differ and may make a contribution. Twin boundaries, however, are special, coherent, boundaries possessing low interfacial energy. An existing bainitic ferrite lath or sheave presents a barrier with interfaces of a different nature.

The expected growth rates were calculated using Thermo-Calc/ Dictra [42], linked with the TCFE12 and MOBFE7 databases, and the Zener-Hillert model [43] for both the nominal (3 wt.%) and low (0.5 wt.%) Mn cases. This loss of Mn content is expected for both TEM thin foils and in LSCM experiments - Fuchs and Berhard recently observed partial Mn depletion up to 9 μm deep in HT-LSCM during austenitisation at 1170 °C for 10 min [44].

For the Dictra simulations, a 1 nm wide ferrite region grew into a 20 mm wide austenite region using the paraequilibrium model for 200 s. For the 3 wt.% Mn and 0.5 wt.% Mn cases interface velocities were obtained of 12 and 22 nm.s^{-1} respectively. Since the actual shape of the growing ferrite plates is neglected this can be considered an underestimate establishing the minimum lengthening rate.

For the Zener-Hillert model the diffusion controlled lengethening rate, v, is given by Eq. (1) below [43].

$$v = \frac{D\Delta G_m^0/V_m}{2\sigma}\frac{x^{\gamma/\alpha}-x^{\gamma 0}}{x^{\gamma 0}-x^{\alpha/\gamma}}\frac{\rho_{cr}}{\rho} \tag{1}$$

Where D is the diffusion coefficient of carbon in austenite, ΔG_m^0 the driving force, V_m is the molar volume, σ is the interfacial energy, ρ_{cr} and ρ are the critical and actual radius of curvature respectivey. The mole fractions of carbon on the austenite side of the interface, the ferrite side of the interface and in the alloy as a whole are given by $x^{\gamma/\alpha}$, $x^{\alpha/\gamma}$ and $x^{\gamma 0}$ respectively.

As in the Dictra simulations the lengthening rate was calculated for the 3 wt.% Mn and 0.5 wt.%Mn cases. In addition, the lengthening rate was calculated on the basis of two extremes of the carbon diffusion coefficient, D_0 and D_{max}. The carbon diffusivity in austenite depends on it mole fraction as in Eq. (2) below [45].

$$D_C^\gamma = 4.53\times 10^{-7}\left(1+x_c(1-x_c)\frac{8339.9}{T}\right)\exp\left[-\left(\frac{1}{T}-2.221\times 10^{-4}\right)(17767-x_c26436)\right] \tag{2}$$

Where x_c is the carbon mole fraction, and T is the temperature.

D_0 is calculated for the nominal alloy composition and D_{max} for the carbon content in the austenite at the interface. Yin et al. [46] note that for low carbon steels the lengthening rate behaviour is not reproduced well by any selection of D but that D_{max} may be expected to display the least deviation. This forms a lower and upper estimate for the expected diffusion controlled lengthening rate according to the Zener-Hillert model.

For 3 wt.% Mn, the calculated lengthening rates are 14.6 nm.s^{-1} and 19,900 nm.s^{-1}. For the 0.5 wt.% Mn, the corresponding lengthening rates are 17.4 and 46,800 nm.s^{-1}. It can be seen that for D_0 the predicted lengthening rate is comparable to that expected from kinetic modelling under paraequilibrium conditions, whilst for D_{max} the rate is significantly higher.

Average tip movement rates measured in the current study generally fall within these two extremes, indicating the growth rate of individual laths is likely to be diffusion controlled. The two examples of very rapid bainitic ferrite growth both exceed the highest lengthening rate calculated for a nominal composition of 3 wt.% Mn, however, due to the limitations imposed by the camera framerate it is impossible to determine if they exceed the calculated rate for the 0.5 wt.% Mn case.

4.3. Thickness

Where possible the mid-length thickness of a lath was measured at the instant that lengthening had ceased. In most cases these fell within 20–150 nm. Several thicker measurements were of textbook appearance sheaves where individual subunits could be identified. Subunit thickness in these sheaves was comparable to that of the individual laths measured. The remaining thicker measurements may therefore also be sheaves but with unfavourable orientation or contrast conditions for viewing subunits. In fact, as noted above one of these sheaves displayed behaviour that appeared consistent with less commonly cited schematics of bainite growth.

Singh et al. [47] developed a quantitative model for plate thickness in Si-rich steels. The most significant variable in determination of plate thickness according to this model was the austenite yield strength, with over 3 times the significance of the driving force which in turn was more significant than the temperature. Van Bohemen [48] likewise developed an empirical model to describe bainite lath thickness as a function of austenite yield strength describing it as an inverse dependence.

A direct comparison of the present observations with these model predictions is complicated by the fact that the present Mn composition and grain size fall outside the range used to derive the austenite yield strength and bainite plate thickness. Furthermore, in the present experiments the microstructure consisted of a mixture of austenite, ferrite and bainite whereas the model was derived from bainitic steels containing a mixture of bainite and austenite [49]. The expected thickness was calculated according to Eq. (3) below, based on the nominal composition and using prior austenite grain sizes of 5, 10 and 20 μm. The calculated thicknesses were 47, 51 and 55 nm respectively. The uncorrected experimentally observed average was 72 ± 2.3 nm. Chang and Bhadeshia [50] apply a stereological correction of 2/π in the measurement of austenite films between bainite plates which was likewise used as a correction for the measurements used by Van Bohemen. Thus the average experimentally observed thickness becomes 45.8 nm, close to that calculated for the smaller austenite grain size.

$$t = \frac{K}{(\sigma_y^\gamma - \sigma_{lim})} \tag{3}$$

Where K is a constant 2 μmMPa and σ_{lim} is given in Eq. (4), for the alloying elements contained in the present steel, below. σ_y^γ was calculated according to Eq. (5) [51] as no term for Mn content was included in the equation given by Van Bohemen.

$$\sigma_{lim} = 66.6+140x_C-1.1x_{Mn}+1.8x_{Si}+7.7x_{Mo}+\frac{4.9}{\sqrt{d^\gamma}} \tag{4}$$

Where x is the alloying element content in wt%, d^γ is the austenite grain size in mm.

$$\sigma_y^\gamma = \left(1-\left(\frac{T_r}{1487-25}\right)^{0.658}\right)\times\left(52.3+47A_C+31.3A_{Si}+1.0A_{Mn}+31.3A_{Mo}+\frac{274}{\sqrt{D^\gamma}}\right) \tag{5}$$

Where A is the alloying element content in at%, D^γ is the austenite grain size in μm and T_r, the quench temperature relative to room temperature, is equal to T-25.

There is variation within the thickness of the bainitic ferrite laths and subunits, with the smallest measured thickness of 24 nm and the largest

148 nm. The average aspect ratio of the laths was 0.07. Wang et al. [52] investigated the aspect ratios of a range of C, Mn, Cr and Si containing steels finding that 90% of measured aspect ratios were below 0.1 with the most common being 0.025. The most comparable composition studied by Wang et al. was Fe-0.5C-3Mn-1.5Si which demonstrated the widest range of aspect ratios (from <0.025 to 0.5). Typically, it might be expected that as the transformation progresses the increase in austenite yield strength as a result of the shrinking austenite grain would tend to reduce lath thickness and aspect ratio [45,46]. However, Ruiz-Jiminez et al. [53] note in high and medium carbon steels containing greater than 1.5wt% Si, the thickness unexpectedly increased as the transformation proceeded, an effect which was correlated with the rate of transformation rather than the state of transformation.

This good agreement between calculated and measured lath thickness indicates that the bainitic ferrite formed during cooling of the thin foils possesses an average thickness and aspect ratio comparable to that found in bulk materials. This indicates that despite the use of a thin foil conditions are similar to that found in the bulk during the growth of bainitic ferrite.

In all cases measured lath thicknesses were within the estimated foil thickness using EELS. In contrast the measured thicknesses for identifiable sheaves are close to, or exceed, the estimated foil thickness. However, several observations indicate that neither the sheaves nor individual laths exist throughout the thickness of the foil. Firstly, Fig. 5 (c) shows a single lath apparently growing across a second bainitic ferrite lath. Secondly, Figs. 7 and 8 clearly show overlap when a growing sheaf impinges on an existing sheaf. Finally, as shown in supplementary video 2, a subunit could be observed to grow above or below, rather than by the side of BF 1. This indicates that the three-dimensional structure of the bainitic ferrite is at least partially maintained despite the highly constricted specimen dimensions.

5. Conclusions

1. Kinetics measurements, measured lath thicknesses, surface relief and orientation relationships are in good agreement with comparable results in the literature from in situ and bulk experiments. Evidence indicates that often a three-dimensional structure for the bainite entity was maintained within the foil.
2. The higher magnification available with the use of TEM allowed more detailed observation of sheaf behaviour and some kinetic measurements of individual subunits. Several examples of behaviour comparable to previously published descriptions of bainite growth were observed when focussing on phenomena at larger length scales.
3. Lengthening behaviour of sheaves was found to be discontinuous, with periods of growth and stasis. In the highest quality observation reported above this could be linked to the behaviour of individual subunits.
4. Variation was found in the lengthening rate. The estimated maximum lengthening rate for regions with very high transformation rate were in excess of 30,000 nm.s^{-1}. The highest quality observations were for bainitic ferrite with lengthening rates in the range of 10–1000 nm.s^{-1}. Most of the measured lengthening rates fall within the range calculated assuming diffusion controlled growth.
5. Laths observed individually displayed comparable lengthening rates and thickness to identified subunits of sheaves.
6. In a small number of cases, the growth of individual laths or subunits was captured from the earliest stages. The lengthening rate was seen to increase after a size of 150–250 nm was reached.
7. Interaction of growing bainitic ferrite laths with twin boundaries was observed. After impingement, growth was observed to continue on the other side of the twin boundary, or to be “reflected” from the boundary depending on relative orientation. A distinct period of stasis was found between periods of growth.

Declaration of Competing Interest

The authors declare that they have no known competing financial interests or personal relationships that could have appeared to influence the work reported in this paper.

Acknowledgments

This work was supported by the Engineering and Physical Sciences Research Council (EPSRC) through the Centre for Doctoral Training in Advanced Metallic Systems (EP/G036950/1). We wish to acknowledge the Henry Royce Institute for Advanced Materials, funded through EPSRC Grants EP/R00661X/1, EP/S019367/1, EP/P02470X/1 and EP/P025285/1, for the financial support and JEOL JEM-F200 access at Royce@Sheffield.

Supplementary materials

Supplementary material associated with this article can be found, in the online version, at doi:10.1016/j.actamat.2023.118924.

References

[1] F.G. Caballero, M.J. Santofimia, C. Garcia-Mateo, J. Chao, C. Garcia de Andres, Theoretical design and advanced microstructure in super high strength steels, Mater. Des. 30 (2009) 2077–2083.
[2] H.K.D.H. Bhadeshia, Bainite in Steels, 3rd ed., Maney Publishing, Leeds, 2015.
[3] F.G. Caballero, H.K.D.H. Bhadeshia, K.J.A Mawella, D.G. Jones, P. Brown, Very strong low temperature bainite, Mater. Sci. Technol. 18 (3) (2002) 279–284.
[4] L.C.D. Fielding, The bainite controversy, Mater. Sci. Technol. 29 (4) (2013) 383–399.
[5] D. Zhang, H. Terasaki, Y. Komizo, In situ observation of phase transformation in Fe-0.15C binary alloy, J. Alloys Compd. 484 (2009) 929–933.
[6] M. Enomoto, T. Sonoyama, H. Yada, Kinetics of austenite to ferrite transformation in 3 mass% Mn low carbon steels, Mater. Trans. JIM 39 (1) (1998) 189–195.
[7] H. Yada, M. Enomoto, T. Sonoyama, Lengthening kinetics of bainitic plates in iron-nickel-carbon alloys, ISIJ Int. 35 (8) (1995) 976–981.
[8] T. Furuhara, S. Abe, G. Miyamoto, Anisotropic Ferrite growth and substructure formation during bainite transformation in Fe-9Ni-C alloys: in-situ measurement, Mater. Trans. 59 (2) (2018) 214–223.
[9] G. Mao, R. Cao, J. Chen, Analysis on bainite transformation in reheated low-carbon bainite weld metals, Mater. Sci. Technol. 33 (15) (2017) 1829–1837.
[10] G. Mao, R. Cao, X. Guo, Y. Jiang, J. Chen, In Situ observation of kinetic processes of lath bainite nucleation and growth by laser scanning confocal microscope in reheated weld metals, Metall. Mater. Trans. A 48A (2017) 5783–5798.
[11] P. Kolmskog, A. Borgenstam, M. Hillert, P. Hedstrom, S.S. Babu, H. Terasaki, Y. Komizo, Direct observation the bainite can grow below M_s, Metall. Mater. Trans. A 43A (2012) 4984–4988.
[12] S. Sainis, H. Farahani, E. Gamsjager, S. van der Zwaag, An in-situ LSCM study on bainite formation in Fe-0.2C-1.5Mn-2.0Cr alloy, Metals (Basel) 8 (2018) 498.
[13] H. Hu, G. Xu, M. Nabeel, N. Dogan, H.S. Zurob, In situ study on interrupted growth behavior and crystallography of bainite, Metall. Mater. Trans. A 52A (2021) 817–825.
[14] Y. Shen, B. Chen, C. Wang, In situ observation and growth kinetics of bainite laths in the coarse-grained heat-affected zone of 2.25Cr-1Mo heat-resistant steel during simulated welding, Metall. Mater. Trans. A 52A (2021) 14–19.
[15] X. Long, F. Zhang, Z. Yang, M. Zhang, Study on bainitic transformation by dilatometer and in situ LSCM, Materials (Basel) 12 (2019) 1534.
[16] J. Tian, G. Xu, L. Wang, M. Zhou, H. Hu, In situ observation of the lengthening rate of bainite sheaves during continuous cooling process in a Fe-C-Mn-Si superbainitic steel, Trans. Indian Inst. Met. 71 (1) (2018) 185–194.
[17] W. Zhou, T. Hou, L. Tao, K. Wu, In Situ observation on the effects of prior martensite formation on nanostructured low-temperature bainite transformation, Metals (Basel) 8 (2018) 818.
[18] G. Xu, F. Liu, L. Wang, H. Hu, A new approach to quantitative analysis of bainitic transformation in a superbainite steel, Scr. Mater. 68 (2013) 833–836.
[19] Z. Hu, G. Xu, H. Hu, L. Wang, Z. Xue, In situ measured growth rates of bainite plates in an Fe-C-Mn-Si superbainitic steel, Int. J. Miner. Metall. Mater. 21 (4) (2014) 371–378.
[20] H. Hu, G. Xu, Y. Zhang, Z. Xue, M. Zhou, Dynamic observation of bainite transformation in Fe-C-Mn-Si superbainite steel, J. Wuhan Univ. Technol.-Mater. Sci. Ed. (2015) 818–821.
[21] M. Nemoto, Growth of bainite in an iron-nickel-carbon alloy, in: High Voltage Electron Microscopy, Academic Press, London, 1974, pp. 230–234.
[22] M. Kang, M.-.X. Zhang, M. Zhu, In situ observation of bainite growth during isothermal holding, Acta Mater. 54 (2006) 2121–2129.
[23] L.S. Darken, R.M. Fisher, Some observations on the growth of pearlite, in: Decomposition of Austenite by Diffusional Processes, Interscience Publishers, New York, 1962, pp. 249–288.

[24] G.R. Purdy, The dynamics of transformation interfaces in steels-I. The ferrite-austenite interface in Fe-C-Mo alloys, Acta Metall. 26 (1978) 477–486.
[25] G.R. Purdy, On the direct observation of the formation of ferrite in steels, Scr. Metall. 21 (1987) 1035–1038.
[26] J. Du, F. Mompiou, W.-.Z. Zhang, In-situ TEM study of dislocation emission associated with austenite growth, Scr. Mater. 145 (2018) 62–66.
[27] M. Onink, F.D. Tichelaar, C.M. Brakman, E.J. Mittemeijer, S. van der Zwaag, An in situ hot stage transmission electron microscopy study of the decomposition of Fe-C austenites, J. Mater. Sci. 30 (1995) 6223–6234.
[28] J. Nutter, H. Farahani, W.M. Rainforth, S. van der Zwaag, Direct TEM observation of α/γ interface migration during cyclic partial phase transformations at intercritical temperatures in an Fe-0.1C –0.5Mn alloy, Acta Mater. 178 (2019) 68–78.
[29] L.C. Chang, H.K.D.H. Bhadeshia, Austenite films in bainitic microstructures, Mater. Sci. Technol. 11 (9) (1995) 874–882.
[30] E.P. Butler, K.F. Hale, Dynamic Experiments in the Electron Microscope, Elsevier/North-Holland Biomedical Press, Amsterdam, 1981, p. 138.
[31] R.F. Egerton, Electron Energy-Loss Spectroscopy in the Electron Microscope, Plenum Press, New York, 1996, pp. 301–307.
[32] W.W. Mullins, The effect of thermal grooving on grain boundary motion, Acta Metall. 6 (1958) 414–427.
[33] D.J. Allen, Thermal Grooving at migrating grain boundaries, Scr. Metall. 16 (1982) 5–9.
[34] J.G. Brons, G.B. Thompson, A comparison of grain boundary evolution during grain growth in fcc metals, Acta Mater. 61 (2013) 3936–3944.
[35] E. Swallow, H.K.D.H. Bhadeshia, High resolution observations of displacements caused by bainitic transformation, Mater. Sci. Technol. 12 (1996) 121–125.
[36] M.J. Peet, H.K.D.H. Bhadeshia, Surface relief due to bainite transformation at 473 K (200 °C), Metall. Mater. Trans. A 42A (2011) 3344–3348.
[37] L.E. Murr, G.I. Wong, R.J. Horylev, Measurement of interfacial free energies and associated temperature coefficients in 304 stainless steel, Acta Metall. 21 (1973) 595–604.
[38] Y. Shibuta, S. Takamoto, T. Suzuki, A molecular dynamics study of the energy and structure of the symmetric tilt boundary of iron, ISIJ Int. 48 (11) (2008) 1582–1591.
[39] H.D.K.H. Bhadeshia, Bainite in Steels: Theory and Practice, Maney Publishing, Leeds, 2015, p. 33.
[40] G.B. Olson, H.K.D.H. Bhadeshia, M. Cohen, Coupled diffusional/displacive transformations, Acta Metall. 37 (2) (1989) 381–389.
[41] J.M. Oblak, R.F. Hehemann, Structure and growth of Widmanstatten ferrite and bainite, in: Transformation and Hardenability in Steels, Climax Molybdenum, Ann Arbor, 1967, pp. 15–30.
[42] J.O. Andersson, T. Helander, L. Höglund, P. Shi, B. Sundman, Thermo-Calc & DICTRA, computational tools for materials science, Calphad 26 (2002) 273–312.
[43] L. Leach, M. Hillert, A. Borgenstam, Modeling C-curves for the growth rate of widmanstatten and bainitic ferrite in Fe-C alloys, Metall. Mater. Trans. A 47A (2016) 19–25.
[44] N. Fuchs, C. Bernhard, Potential and limitations of direct austenite grain growth measurement by means of HT-LSCM, Mater. Today Commun. 28 (2021), 102468.
[45] J. Ågren, A revised expression for the diffusivity of carbon in binary Fe-C austenite, Scr. Metall. 20 (1986) 1507–1510.
[46] J. Yin, L. Leach, M. Hillert, A. Borgenstam, C-Curves for lengthening of widmanstatten and bainitic ferrite, Metall. Mater. Trans. A 48A (2017) 3997–4005.
[47] S.B. Singh, H.K.D.H. Bhadeshia, Estimation of bainite plate-thickness in low-alloy steels, Mater. Sci. Eng. A 245 (1998) 72–79.
[48] S.M.C. van Bohemen, Exploring the correlation between the austenite yield strength and the bainite lath thickness, Mater. Sci. Eng. A 731 (2018) 119–123.
[49] C. Garcia-Mateo, F.G. Caballero, H.K.D.H. Bhadeshia, Acceleration of low-temperature bainite, ISIJ Int. 43 (2003) 1821–1825.
[50] L.C. Chang, H.K.D.H. Bhadeshia, Austenite films in bainitic microstructures, Mater. Sci. Technol. 11 (9) (1995) 874–882.
[51] A. Eres-Castellanos, I. Toda-Caraballo, A. Latz, F.G. Caballero, C. Garcia-Mateo, An integrated-model for austenite yield strength considering the influence of temperature and strain rate in lean steels, Mater. Des. 188 (2020), 108435.
[52] J. Wang, S. van der Zwaag, Z. Yang, H.-.S. Fang, Aspect ratio of bainite in steels, Mater. Lett. 45 (2000) 228–234.
[53] V. Ruiz-Jimenez, J.A. Jimenez, F.G. Caballero, C. Garcia-Mateo, Bainitic ferrite plate thickness evolution in two nanostructured steels, Materials (Basel) 14 (2021) 4347.